ACCSCIENCE PUBLISHING

Tumor Discovery

ORIGINAL RESEARCH ARTICLE

# Integration of habitat and peritumoral radiomics for predicting esophagotracheal fistula in esophageal cancer patients post-radiotherapy

**Zhuomiao Ye[1,2†], Fei Xie[3†], Longbin Zhang[4†], YiQing Zhao[5†], Chao Deng[3*], and Mingzhu Yin[1,2*]**

[1]Clinical Research Center, Medical Pathology Center, Cancer Early Detection and Treatment Center and Translational Medicine Research Center, Chongqing University Three Gorges Hospital, Chongqing University, Wanzhou, Chongqing, China

[2]School of Medicine Chongqing University, Chongqing University, Shapingba, Chongqing, China

[3]Department of Breast Surgery, Chongqing University Three Gorges Hospital, Chongqing University, Wanzhou, Chongqing, China

[4]Cancer Center, Chongqing University Three Gorges Hospital, Chongqing, China

[5]Department of Oncology, Shuguang Hospital Affiliated to Shanghai University of Traditional Chinese Medicine, Shanghai, China

*†These authors contributed equally to this work.*

***Corresponding authors:**
Chao Deng
(dengchao0715@126.com)
Mingzhu Yin
(yinmingzhu2008@126.com)

**Citation:** Ye Z, Xie F, Zhang L, Zhao Y, Deng C, Yin M. Integration of habitat and peritumoral radiomics for predicting esophagotracheal fistula in esophageal cancer patients post-radiotherapy. *Tumor Discov*. 2025;4(4):123-134. doi: 10.36922/TD025180030

**Received:** April 28, 2025

**Revised:** May 23, 2025

**Accepted:** May 30, 2025

**Published online:** June 30, 2025

**Copyright:** © 2025 Author(s). This is an Open-Access article distributed under the terms of the Creative Commons Attribution License, permitting distribution, and reproduction in any medium, provided the original work is properly cited.

**Publisher's Note:** AccScience Publishing remains neutral with regard to jurisdictional claims in published maps and institutional affiliations.

## Abstract

Esophageal cancer is a prevalent and lethal malignancy, particularly in Asian countries. Esophagotracheal fistula (ETF) is a severe complication that significantly impacts patient survival and quality of life. This study aims to develop a radiomics model based on habitat and peritumoral analysis to predict ETF occurrence in esophageal cancer patients following radiotherapy. We conducted a retrospective study involving 120 esophageal cancer patients treated between January 2018 and December 2022. We utilized computed tomography imaging data to perform habitat and peritumoral radiomics analyses. The study cohort was divided into a training set ($n$ = 84) and a validation set ($n$ = 36). Models were constructed using machine learning algorithms, and their performance was evaluated using the area under the receiver operating characteristic curve area under the curve (AUC), calibration curves, and decision curve analysis. The habitat-based radiomics model achieved superior predictive performance with an AUC of 0.831 in the test cohort, outperforming conventional radiomics and clinical models. The integration of habitat features, peritumoral radiomics, and clinical risk factors resulted in a comprehensive model with excellent discriminatory ability and calibration. Habitat analysis revealed distinct subregions within tumors, with specific habitats correlating strongly with ETF development. Our study demonstrates the potential of habitat and peritumoral radiomics in predicting ETF in esophageal cancer patients undergoing radiotherapy. The developed Combined model, integrating advanced radiomics features and clinical factors, provides a promising tool for individualized risk stratification and treatment planning. Future research should focus on prospective validation and the incorporation of multimodal imaging to enhance predictive accuracy.

***Keywords:*** Esophageal cancer; Radiomics; Esophagotracheal fistula; Habitat analysis; Peritumoral radiomics

## 1. Introduction

Esophageal cancer ranks among the most prevalent and lethal malignancies worldwide, with epidemiological data revealing significant regional variations in incidence rates. Asian countries, particularly China, exhibit a higher prevalence of the disease, especially esophageal squamous cell carcinoma.[1,2] Clinically, patients with esophageal cancer often present with dysphagia, weight loss, chest pain, and food reflux. These symptoms are particularly pronounced in advanced stages, severely impacting quality of life.[3] Computed tomography (CT) plays a crucial role in diagnosing esophageal cancer, providing essential information about tumor size, location, and lymph node metastasis, especially during preoperative staging.[4]

Radiomics, an emerging technology in oncology, aims to extract tumor characteristics through quantitative analysis of medical imaging data, thereby aiding in the assessment of tumor biological behavior and prognosis.[5] Its strength lies in the ability to extract high-dimensional data from routine imaging, which can then be analyzed using machine learning methods to reveal relationships between tumor biological properties and clinical outcomes.[6] Radiomics not only enhances diagnostic accuracy for tumors but also provides a basis for personalized treatment, supporting clinical decision-making.[7] In recent years, radiomics has shown promising prospects in esophageal cancer research, assisting physicians in making more precise judgments in complex clinical settings.

Esophagotracheal fistula (ETF), a complication of esophageal cancer, typically results from tumor erosion through the esophageal wall into the trachea.[8] The invasive growth of the tumor can disrupt the normal structure between the esophagus and trachea, forming a fistulous tract. The pathophysiological mechanism primarily involves local tumor infiltration and tissue ischemic necrosis, leading to the formation of an abnormal channel between the trachea and esophagus, subsequently causing severe complications such as recurrent aspiration pneumonia and malnutrition.[3] Additionally, chronic inflammation and post-radiotherapy tissue changes may contribute to fistula formation.[9] The occurrence of ETF not only exacerbates patient morbidity but also significantly reduces survival rates,[9] underscoring the importance of early detection and intervention.

Imaging examinations are crucial in evaluating ETF, with commonly used techniques including X-ray, CT, and magnetic resonance imaging.[10] Identification of characteristic imaging features helps clinicians determine the specific location and morphology of the fistula and its relationship with surrounding structures, thus guiding surgical intervention or other treatment modalities. According to existing literature, typical imaging manifestations of ETF include contrast agent leakage into the trachea, gas accumulation, and abnormal esophageal dilation. A close correlation exists between imaging features and clinical presentations.[11,12]

This study aims to investigate the relevant imaging features of esophageal cancer and its complication, ETF, and to analyze their underlying pathophysiological mechanisms using radiomics approaches. This article will begin with an overview of the epidemiology and clinical manifestations of esophageal cancer, followed by an exploration of the pathophysiological mechanisms of ETF, and finally, discusses the application and importance of radiomics in oncology. This research seeks to provide insights and references for researchers in related fields.

## 2. Materials and methods

### 2.1. Study population

This retrospective study included 120 patients treated at Chongqing University Three Gorges Hospital between January 2018 and December 2022. Inclusion criteria were: (1) pathologically confirmed esophageal malignancy; (2) no prior surgery and received radiotherapy at our institution; (3) enhanced CT examination before radiotherapy at our hospital. Exclusion criteria were: (1) poor CT image quality; (2) incomplete clinical or imaging data; (3) lesions with a maximum diameter of <1 cm; (4) pre-existing ETF before radiotherapy. The staging was performed according to the Tumor-Node-Metastasis (TNM) staging system described in the 8$^{th}$ edition of the American Joint Committee on Cancer manual.[13] Patients suspected of ETF were definitively diagnosed using esophageal barium contrast radiography.

The final cohort of 120 patients was randomly divided into a training set ($n$ = 84) and an internal validation set ($n$ = 36) in a 7:3 ratio. This study was approved by the institutional ethics committee, with a waiver of informed consent. Collected clinical data included sex, age, presence of esophageal ulcer, number of radiation fractions, gross tumor volume (GTV) dose, TNM stage, involvement of the mesothoracic or upper thoracic esophagus, chemotherapy, chemoimmunotherapy, Karnofsky performance status (KPS), height, and weight. Patient characteristics are presented in Table 1.

### 2.2. Image acquisition and preprocessing

All patients underwent contrast-enhanced CT scanning prior to radiotherapy for treatment planning and target volume delineation. The enhanced CT images were used for GTV contouring and subsequent radiotherapy planning. Pre-radiotherapy images were acquired using United

**Table 1. Baseline demographic and clinical characteristics of the patients**

| Feature | Train set | | | | Test set | | | |
|---|---|---|---|---|---|---|---|---|
| | All | Non-ETF | ETF | *p* | All | Non-ETF | ETF | *p* |
| Age (years) | 63.50±7.92 | 62.35±7.59 | 65.38±8.21 | 0.089 | 66.06±7.08 | 65.88±7.14 | 66.45±7.27 | 0.810 |
| Number of radiation (*n*) | 28.55±2.68 | 28.19±3.04 | 29.12±1.88 | 0.039 | 28.47±3.12 | 28.40±3.44 | 28.64±2.38 | 0.896 |
| GTV dose (Gy) | 59.80±6.22 | 58.74±7.00 | 61.52±4.27 | 0.007 | 59.69±7.36 | 60.14±7.44 | 58.66±7.42 | 0.410 |
| KPS (score) | 82.02±9.79 | 83.56±11.65 | 79.53±4.81 | 0.041 | 83.33±9.02 | 86.40±8.23 | 76.36±6.74 | 0.002 |
| Height (cm) | 159.30±7.67 | 158.75±8.58 | 160.19±5.92 | 0.062 | 156.39±7.97 | 155.80±7.07 | 157.73±9.98 | 0.512 |
| Weight (kg) | 56.15±43.47 | 59.00±55.00 | 51.52±6.92 | 0.974 | 60.73±65.92 | 65.42±79.02 | 50.09±6.66 | 0.986 |
| Sex (*n*) | | | | | | | | |
| Female | 25 (29.76) | 21 (40.38) | 4 (12.50) | 0.014 | 13 (36.11) | 11 (44.00) | 2 (18.18) | 0.267 |
| Male | 59 (70.24) | 31 (59.62) | 28 (87.50) | | 23 (63.89) | 14 (56.00) | 9 (81.82) | |
| Esophageal ulcer | | | | | | | | |
| No | 41 (48.81) | 32 (61.54) | 9 (28.12) | 0.006 | 18 (50.00) | 14 (56.00) | 4 (36.36) | 0.469 |
| Yes | 43 (51.19) | 20 (38.46) | 23 (71.88) | | 18 (50.00) | 11 (44.00) | 7 (63.64) | |
| T stage | | | | | | | | |
| T2 | 29 (34.52) | 17 (32.69) | 12 (37.50) | 0.568 | 17 (47.22) | 12 (48.00) | 5 (45.45) | 0.860 |
| T3 | 40 (47.62) | 27 (51.92) | 13 (40.62) | | 11 (30.56) | 7 (28.00) | 4 (36.36) | |
| T4 | 15 (17.86) | 8 (15.38) | 7 (21.88) | | 8 (22.22) | 6 (24.00) | 2 (18.18) | |
| N stage | | | | | | | | |
| N0 | 14 (16.67) | 13 (25.00) | 1 (3.12) | 0.042 | 12 (33.33) | 11 (44.00) | 1 (9.09) | 0.013 |
| N1 | 58 (69.05) | 33 (63.46) | 25 (78.12) | | 15 (41.67) | 11 (44.00) | 4 (36.36) | |
| N2 | 11 (13.10) | 6 (11.54) | 5 (15.62) | | 8 (22.22) | 2 (8.00) | 6 (54.55) | |
| N3 | 1 (1.19) | 0 | 1 (3.12) | | 1 (2.78) | 1 (4.00) | 0 | |
| M stage | | | | | | | | |
| M0 | 66 (78.57) | 41 (78.85) | 25 (78.12) | 0.923 | 33 (91.67) | 23 (92.00) | 10 (90.91) | 0.935 |
| M1 | 18 (21.43) | 11 (21.15) | 7 (21.88) | | 3 (8.33) | 2 (8.00) | 1 (9.09) | |
| Mesothoracic esophagus | | | | | | | | |
| No | 42 (50.00) | 28 (53.85) | 14 (43.75) | 0.500 | 19 (52.78) | 14 (56.00) | 5 (45.45) | 0.825 |
| Yes | 42 (50.00) | 24 (46.15) | 18 (56.25) | | 17 (47.22) | 11 (44.00) | 6 (54.55) | |
| Upper thoracic esophagus | | | | | | | | |
| No | 66 (78.57) | 40 (76.92) | 26 (81.25) | 0.845 | 25 (69.44) | 19 (76.00) | 6 (54.55) | 0.371 |
| Yes | 18 (21.43) | 12 (23.08) | 6 (18.75) | | 11 (30.56) | 6 (24.00) | 5 (45.45) | |
| Chemotherapy | | | | | | | | |
| No | 22 (26.19) | 10 (19.23) | 12 (37.50) | 0.111 | 12 (33.33) | 6 (24.00) | 6 (54.55) | 0.159 |
| Yes | 62 (73.81) | 42 (80.77) | 20 (62.50) | | 24 (66.67) | 19 (76.00) | 5 (45.45) | |
| Chemotherapy and immunotherapy | | | | | | | | |
| No | 73 (86.90) | 47 (90.38) | 26 (81.25) | 0.383 | 32 (88.89) | 24 (96.00) | 8 (72.73) | 0.141 |
| Yes | 11 (13.10) | 5 (9.62) | 6 (18.75) | | 4 (11.11) | 1 (4.00) | 3 (27.27) | |

Notes: Data are presented as number of subjects (percentage). Numbers in brackets represent the percentage of subjects within each group.
Abbreviations: ETF: Esophagotracheal fistula; GTV: Gross tumor volume; KPS: Karnofsky Performance Status.

Imaging uCT 760 (United Imaging Medical Technology, China) and Philips Brilliance 64 slice CT scanner (Philips Medical Systems, Netherlands). Scanning parameters included a tube voltage of 120 kVp, automatic tube current modulation (200 – 400 mA), and a slice thickness of 1.0 – 1.5 mm. Images were reconstructed using iterative reconstruction techniques and stored in DICOM format. To enhance consistency and robustness in radiomic feature

extraction stability, the following preprocessing steps were applied: (1) N4 bias field correction; (2) voxel resampling to an isotropic resolution of 1 × 1 × 1 $mm^3$; (3) gray-level normalization, with Hounsfield Unit values limited to −1200 – 600 range.

### 2.3. Workflow of radiomics analysis

Radiomics analysis was conducted through a series of steps, including image segmentation, feature extraction, feature selection, model construction, and performance evaluation (Figure 1). Two primary model construction approaches were employed: habitat analysis and peritumoral region dilation. These were ultimately compared and integrated with clinical and intratumoral models.

### 2.4. Region of interest (ROI) segmentation

The ROIs were delineated from pre-radiotherapy GTV, independently segmented by two experienced radiation oncologists. The delineations were imported into ITK-SNAP software (version 3.8.0, www.itksnap.org) for confirmation and minor adjustments by both physicians. All ROIs were subsequently reviewed by a senior radiation oncologist with over 20 years of experience. Any discrepancies identified were discussed and resolved prior to final acceptance, ensuring the accuracy and clinical reliability of the segmentation. To assess inter-observer reproducibility, a random sample of 30 cases was selected, and the intraclass correlation coefficient (ICC) was calculated for all extracted radiomic features to evaluate the feature-level agreement. An ICC ≥0.85 was considered indicative of excellent reproducibility. This sample size and methodology align with recent standards in habitat radiomics studies.[14-17]

### 2.5. Peritumoral region dilation

The Mask Padding Toolkit provided by the Onekey AI platform (Version 3.3.17, China) was used to extend the ROIs. A radial interval of 1 mm was configured to explore the impact of different extension distances on model prediction accuracy. Any ROI extensions beyond the esophageal tumor lesion or overlapping with organs—such as lungs, trachea, blood vessels, heart, or diaphragm—were manually adjusted.

### 2.6. Habitat analysis

Local image features, including entropy and energy values, were extracted from each voxel within the volume of interest (VOI) to characterize the tumor microenvironment based on CT imaging. Prior to habitat characterization, all intensity features were registered. We employed the

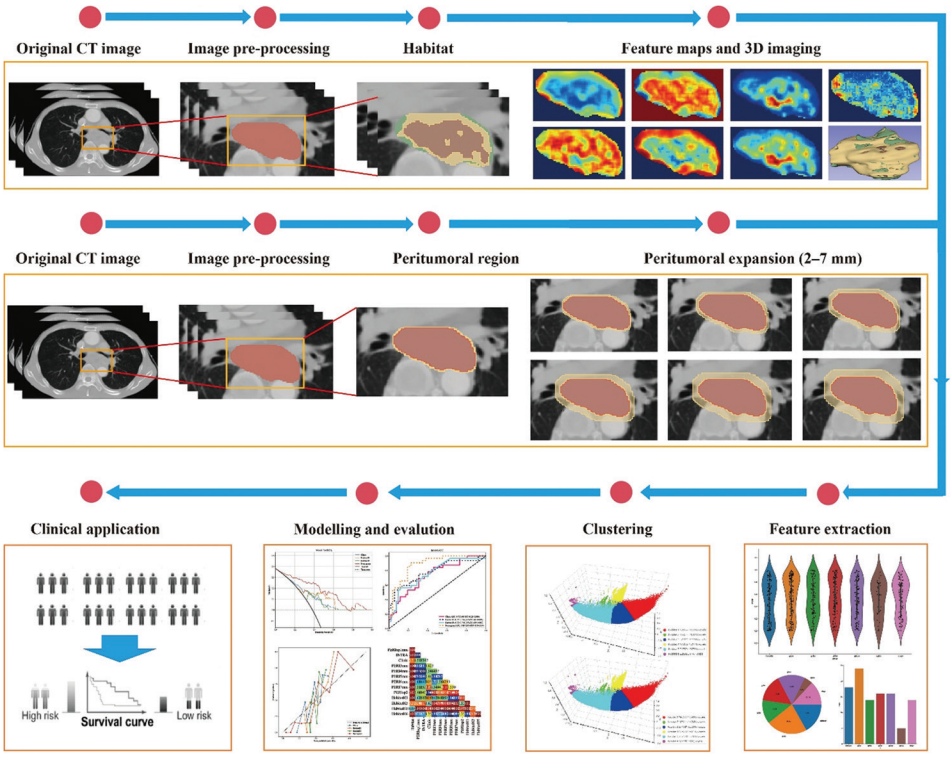


**Figure 1.** Workflow of radiomics analysis
Abbreviation: CT: Computed tomography.

K-means module from scikit-learn python (https://scikit-learn.org/stable/index.html) to cluster habitat subregions. Individual voxels in each cluster were grouped based on local similarity using a queue-based K-means algorithm, with squared Euclidean distance as the similarity metric. All voxels were assigned to one of the clusters and visualized as spatial habitats in the original image space. The optimal number of clusters was determined using the Calinski-Harabasz (CH) index,[18] with cluster numbers ranging from 2 to 7.

### 2.7. Feature extraction and selection

Radiomics features were extracted using PyRadiomics (version 3.0.1, USA), including shape-based features, first-order features, texture features, and wavelet-transformed features. Features were extracted from the whole tumor, habitat subregions, and peritumoral regions. Feature selection steps included: (1) Z-score normalization; (2) t-test to screen significant features ($p<0.05$); (3) Spearman correlation analysis to remove highly correlated features ($|r| >0.9$); (4) minimum redundancy maximum relevance algorithm for feature ranking; (5) Least Absolute Shrinkage and Selection Operator (LASSO) regression to select features with non-zero coefficients corresponding to the optimal $\lambda$ value.

### 2.8. Model construction and evaluation

Five models were constructed: (1) an intratumoral radiomics model (INTRA); (2) a peritumoral radiomics model; (3) a habitat radiomics model; (4) a clinical feature-based model; (5) a fusion model integrating radiomics and clinical features. Machine learning algorithms employed included logistic regression, support vector machine (SVM), k-nearest neighbors, random forest, extremely randomized trees (ET), extreme gradient boosting (XGBoost), light gradient boosting machine (LightGBM), and multi-layer perceptron. Model performance was evaluated using receiver operating characteristic curves, calibration curves, and decision curve analysis (DCA). The DeLong test was used to compare the area under the curve (AUC) values across models. Specific hyperparameter configurations for each model are detailed in Table S1. All models adhered to a consistent data preprocessing pipeline.

### 2.9. Statistical analysis

Statistical analyses were performed using Python (version 3.7.6, Python Software Foundation, United States) and R (version 4.0.3, The R Foundation for Statistical Computing, Austria). The Shapiro-Wilk test was used to verify the normality of clinical features. Continuous variables were compared using the Mann-Whitney U test depending on their distribution characteristics, while categorical variables were compared using Chi-squared ($\chi^2$) tests or Fisher's exact tests. A $p<0.05$ was considered statistically significant.

## 3. Results

### 3.1. Patient characteristics

This study included 120 esophageal cancer patients from our hospital, who were randomly divided into a training group ($n$ = 84) and a validation group ($n$ = 36). Among these patients, 43 developed ETF following radiotherapy. Patients were censored at the date of last follow-up or at death from other causes. The median follow-up duration was 11.8 months (range: 1.6 – 72.6 months). Detailed clinical characteristics are presented in Table 1. Univariate analysis (Table S2 and Figure S1) identified several factors associated with post-radiotherapy ETF, including chemotherapy (odds ratio [OR] = 0.476, 95% confidence interval [CI]: 0.305 – 0.745, $p$=0.006), T_stage (OR = 0.852, 95% CI: 0.751 – 0.968, $p$=0.038), number_of_radiation fractions (OR = 0.984, 95% CI: 0.971 – 0.997, $p$=0.044), height (OR = 0.997, 95% CI: 0.995 – 0.999, $p$=0.034), and KPS (OR = 0.994, 95% CI: 0.989 – 0.998, $p$=0.019). Other factors such as GTV_dose ($p$=0.051) and age ($p$=0.052) approached statistical significance. In the multivariate analysis (Table S3 and Figure S2), KPS (OR = 0.924, 95% CI: 0.876 – 0.975, $p$=0.004) remained strongly associated with ETF occurrence. Additionally, although GTV dose (OR = 1.054, 95% CI: 0.998 – 1.113, $p$=0.061) and chemotherapy (OR = 0.436, 95% CI: 0.174 – 1.091, $p$=0.076) were not significant, both demonstrated strong trends, suggesting potential clinical relevance. Specifically, increased GTV dose appeared to be associated with higher ETF risk, while patients receiving chemotherapy showed a trend toward reduced ETF occurrence risk.

These findings suggest that patients with higher KPS scores had a lower risk of developing ETF. To assess potential multicollinearity in the multivariable model, we calculated the variance inflation factor (VIF) and the correlation coefficient matrix (Figure S3 and Table S4). All included variables had VIF values <2 (range: 1.02 – 1.58), which is well below the commonly used threshold of 5, indicating no significant multicollinearity in the model. Correlation analysis showed that, except for a moderate negative correlation between upper thoracic esophagus and mesothoracic esophagus (r = −0.55), all other correlations had absolute values below 0.3, further confirming the relative independence of the variables in the model.

### 3.2. Sub-region cluster and feature selection

We characterized the GTV region using 19 imaging features, with the delineation effectiveness of each feature

shown in Figure 2. The optimal number of clusters was determined to be six based on the CH score. Six distinct habitats (H1-H6) were identified within each tumor, with the following average (from highest to lowest): H3 (32.03%), H5 (18.78%), H1 (16.93%), H4 (15.11%), H2 (14.33%), and H6 (2.81%). Following Yuan's method,[14] we established intra-tumor heterogeneity (ITH) scores to quantify heterogeneity across tumor regions. Logistic regression analysis of these habitat features in relation to ETF showed positive correlations for H1, H3, and H5, while H6 exhibited an overall negative correlation (Figure S4). Analysis across axial, sagittal, and coronal planes revealed that H1, corresponding to the outermost tumor region, had the strongest association with ETF occurrence, followed by H3 and H5, which corresponded to the middle and innermost tumor regions, respectively (Figure 3). In contrast, H2 and H4 did not demonstrate significant associations with ETF occurrence in the multivariate analysis. Therefore, to enhance model parsimony and predictive performance, we included only the statistically significant habitats (H1, H3, H5, and H6) and their associated radiomics features in the final habitat

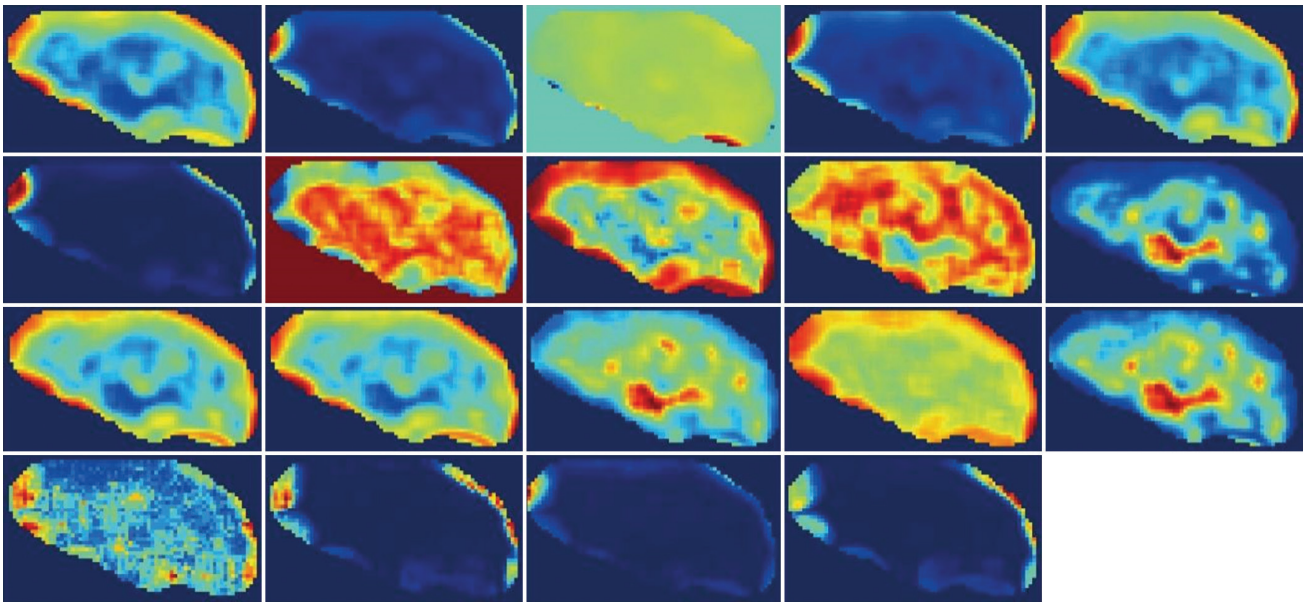

**Figure 2.** Visualization of the delineation effectiveness of 19 imaging features for defining gross tumor volume

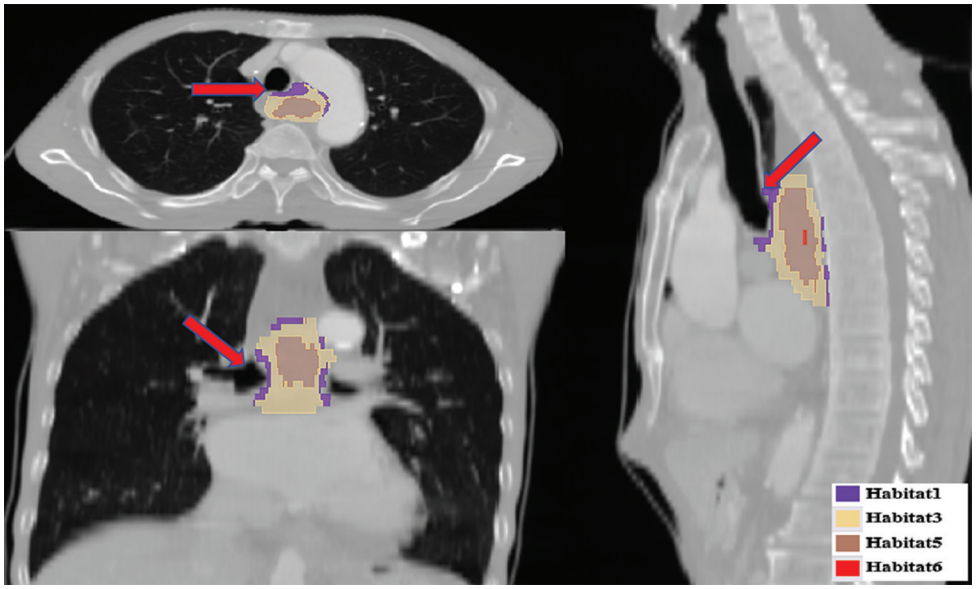


**Figure 3.** Visualization of different habitat regions within the gross tumor volume

model. This selection process ensured that each variable included in the model made an independent contribution to ETF risk prediction, thereby improving the overall performance and clinical utility of the model.

A total of 1,789 handcrafted radiomics features were extracted from each CT image set. For habitat analysis, an average of 24,579 local features per tumor were derived from voxel-wise characterization within the GTV. The most stable and predictive features were selected using the LASSO regression method with 10-fold cross-validation.

### 3.3. Performance and comparison of signatures

#### *3.3.1. Habitat radiomics models*

The habitat-based radiomics model demonstrated excellent predictive performance for ETF across both cohorts. In the training set, it achieved an AUC of 0.846 (95% CI: 0.761 – 0.930). The model maintained robust performance in the test set, with an AUC of 0.822 (95% CI: 0.679 – 0.983). Performance varied across individual habitat regions, with H1 and H3 showing similar results in both the training and test sets. H1 achieved an AUC of 0.725 (95% CI: 0.558 – 0.893) in the test set, while H3 achieved an AUC of 0.795 (95% CI: 0.649 – 0.940). These values were lower than the integrated habitat model (Habitat), which combined features from H1, H3, H5, and H6. AUC values for individual habitat subregions in the test set are presented in Figure S5.

#### *3.3.2. Peritumoral models*

Eight peritumoral models were developed based on different expansion intervals (1 mm, 2 mm, 3 mm, 4 mm, 5 mm, 6 mm, and 7 mm) and their combinations (Figure 4). Among the individual models, the 2-mm peritumoral expansion model (PERI2 mm) exhibited the highest predictive performance, achieving AUCs of 0.954 in the training set and 0.709 in the test set. The combined peritumoral model (PERICombined), integrating features from all expansion intervals, achieved an AUC of 0.745 (95% CI: 0.582 – 0.909) in the test set.

#### *3.3.3. Clinical model and intratumoral models*

The clinical model, constructed using an SVM classifier and incorporating all available clinical information, showed moderate predictive performance. In the test set, it achieved an AUC of 0.697 (95% CI: 0.564 – 0.830). Similarly, the INTRA, also constructed using an SVM classifier, performed well in the training set with an AUC of 0.976 (95% CI: 0.952 – 1.000). This model maintained its performance in the test set (AUC 0.660, 95% CI: 0.478 – 0.842).

#### *3.3.4. Combined model*

To optimize predictive performance, we developed a comprehensive model (Combined), incorporating habitat radiomics, peritumoral radiomics, intratumoral radiomics, and clinical characteristics. After comparing different machine learning algorithms, we found that SVM demonstrated the best overall performance. This combined model demonstrated excellent performance, achieving the highest AUC values of 0.925 (95% CI: 0.867 – 0.983) and 0.831 (95% CI: 0.679 – 0.983) in the training and validation sets, respectively. We compared 16 models constructed using SVM classifiers, with results for training and test sets shown in Figure 5. The Combined model was compared separately with the Habitat model, INTRA model, and PERICombined model (Table S5 and Figure S6), consistently demonstrating superior predictive performance. Using the Combined model, patients were stratified into high-risk and low-risk groups for ETF following radiotherapy. Follow-up analysis showed a significant difference in overall survival (OS) between the two groups ($p$=0.0077), as shown in Figure S7. A detailed comparison of the predictive performance of the five models in both the training and testing sets is provided in Table S5.

To further elucidate the relationship between risk stratification and OS, we performed a landmark analysis using a 5-month time point after radiotherapy—corresponding to the average time to ETF occurrence in our cohort and consistent with previous reports. Patients

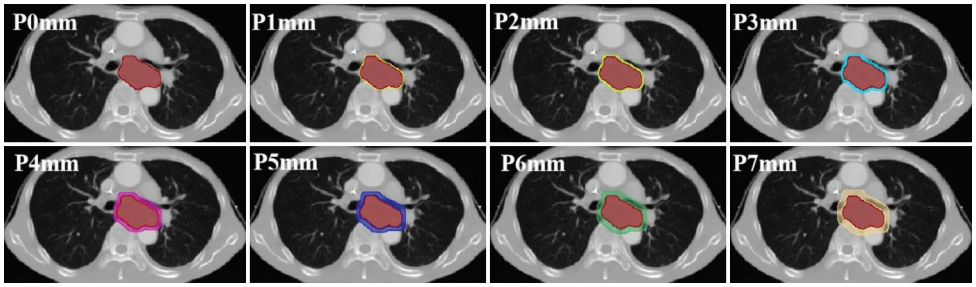


**Figure 4.** Visualization of different expansion intervals on gross tumor volume

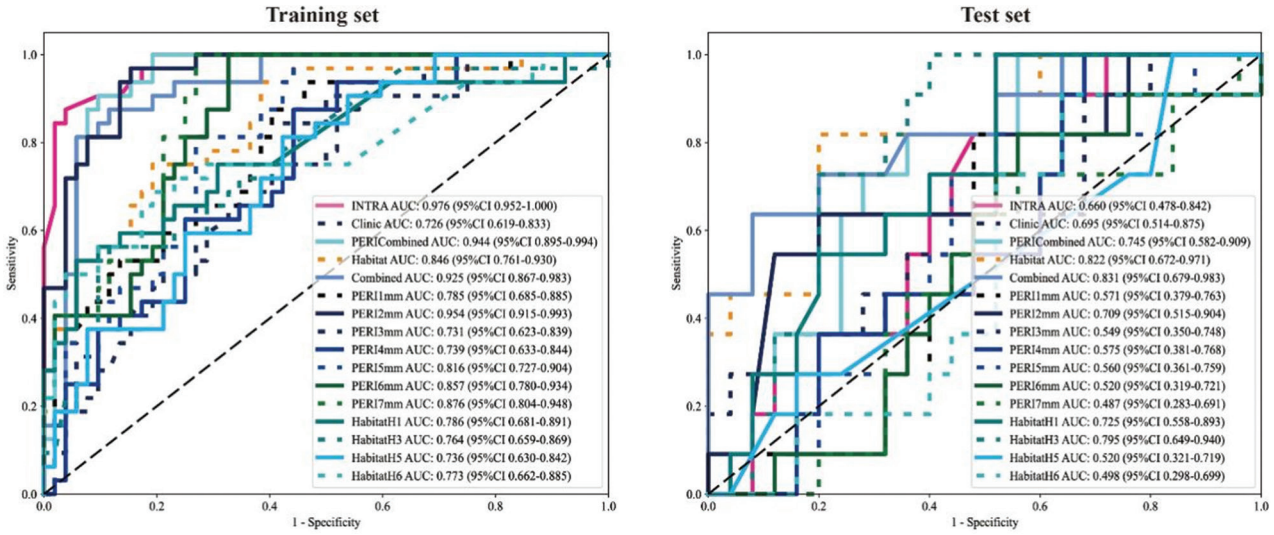


**Figure 5.** Receiver operating characteristic curves comparing the performance of 16 predictive models in the training and test sets. Model performance is quantified by area under the curve with 95% confidence intervals shown in the legend.

were grouped into high-risk and low-risk categories according to the combined model prior to treatment. Before the 5-month landmark, there was no statistically significant difference in OS between the high-risk and low-risk groups (log-rank $p$=0.91), indicating comparable early survival outcomes. In contrast, after the 5-month landmark, the OS difference became statistically significant (log-rank $p$=0.002), with the high-risk group showing markedly worse survival (Figure S8). This suggests that the prognostic value of the combined model is primarily reflected in long-term outcomes, particularly following the typical window of ETF development.

### *3.3.5. Calibration, DeLong test, and DCA*

Calibration curves were constructed using the Hosmer-Lemeshow test to assess model goodness-of-fit. The Combined model displayed better calibration than other models across all cohorts, indicating consistency between predicted and observed probabilities (Figure S9). The DeLong test was utilized to compare the AUC of different models (Figure S10). We also conducted DCA to evaluate the clinical utility of the predictive models (Figure S11). Details on the calibration curves, DeLong test, and DCA are provided in (Figures S9-S11). Compared to other models, the combined model exhibited superior net benefit across a wide range of threshold probabilities in both training and test sets. This suggests that the combined model has the highest clinical value in predicting ETF occurrence in esophageal cancer patients undergoing radiotherapy.

Overall, our comprehensive analysis of CT-based predictive models for ETF in esophageal cancer patients receiving radiotherapy demonstrates that the habitat radiomics model outperforms other single-feature models. The Combined model integrating multiple radiomics features and clinical factors exhibits the best overall performance and clinical utility. These results suggest that our non-invasive, CT-based nomogram model holds significant promise as a decision-support tool for identifying high-risk patients and guiding personalized treatment strategies in the context of radiotherapy for esophageal cancer.

## 4. Discussion

This study developed and validated a radiomics-based model integrating habitat and peritumoral analyses to predict the occurrence of ETF in esophageal cancer patients following radiotherapy. The habitat-based radiomics model outperformed conventional radiomics and clinical models, achieving an AUC of 0.831 in the test cohort. Among the standalone radiomics models, the Habitat model significantly surpassed other single radiomics models. By integrating habitat features, peritumoral radiomics, and clinical risk factors, we constructed a comprehensive model that achieved excellent discriminatory power (AUC = 0.831) and calibration, making it suitable for individualized ETF risk prediction.

In the multivariate analysis, the KPS score was significantly and negatively correlated with the occurrence of ETF after radiotherapy, indicating that patients with poorer performance status are more likely to develop ETF. This finding is consistent with previous literature, as a lower KPS score usually reflects reduced overall

resistance and repair capacity, making these patients more susceptible to serious treatment-related complications such as ETF. Therefore, for such high-risk patients, enhanced monitoring and supportive care are warranted, especially during chemoradiotherapy. Although GTV dose and chemotherapy did not reach conventional statistical significance, both showed strong trends. An increased GTV dose was associated with a higher risk of ETF, which may be related to more severe local tissue damage caused by high-dose radiotherapy to the tumor and surrounding normal tissues. The literature widely acknowledges that local tissue damage from radiotherapy is a key mechanism in the development of ETF.[19,20] Radiotherapy can cause necrosis of the tumor and adjacent tracheal and esophageal tissues, and if timely repair does not occur, a fistula will likely develop. Choi *et al.*[20] reported that about 28.8% of ETF cases were related to cancer treatment rather than tumor progression. Balazs *et al.*[21] also found that the peak incidence of ETF occurred approximately 4.4 months after radiotherapy, suggesting a delayed effect of treatment-related tissue injury. Therefore, patients receiving high-dose radiotherapy should be closely monitored, especially within a 3 – 6 month window after treatment, for early detection and intervention of ETF. In this study, chemotherapy showed a trend toward reducing the risk of ETF, which may be related to tumor shrinkage, reduced local pressure, and the synergistic effect of radiotherapy. However, some studies have indicated that neoadjuvant chemoradiotherapy or immunotherapy can also induce ETF due to treatment-induced tumor necrosis and impaired tissue repair.[22,23] Currently, there is no consensus on whether radiotherapy or chemotherapy is more likely to cause ETF, but most viewpoints suggest that local damage from radiotherapy plays a more prominent role.

Habitat analysis is an emerging technique in biomedical research aimed at revealing tumor pathophysiology through a comprehensive analysis of multidimensional features of the tumor microenvironment.[24] Habitat imaging divides tumors into distinct subregions based on imaging features, providing a more comprehensive assessment of intratumoral heterogeneity than whole-tumor radiomics.[25] In our study, we identified four habitat subregions—H1, H3, H5, and H6—within esophageal tumors, potentially corresponding to areas at different distances from the tumor surface. H1—representing the outermost tumor region adjacent to the trachea—demonstrated the strongest association with ETF occurrence. This finding aligns with the anatomical proximity of the esophageal tumor surface to the trachea, a critical factor in fistula formation. H3 and H5, which occupy larger volumes within the tumor and extend toward the tumor periphery, also showed significant associations with ETF risk, potentially reflecting their involvement in structural compromise of the surrounding tissue. In contrast, H6, located in the tumor core and representing a smaller volume, exhibited minimal correlation with ETF development.

The superiority of the habitat-based model over conventional radiomics suggests that the spatial heterogeneity captured by habitat analysis provides more relevant information for ETF prediction. This aligns with findings by Bi *et al.*,[15] who demonstrated that habitat radiomics outperformed whole-tumor analysis in predicting platinum resistance in ovarian cancer. Similarly, Caii *et al.*[26] showed improved predictive accuracy for immunotherapy response in non-small cell lung cancer (NSCLC) by combining habitat radiomics with deep learning, reinforcing its potential for personalized immunotherapy management.

Peritumoral analysis holds significant clinical importance in tumor prognosis assessment. Extracting imaging features from the tumor and its surrounding tissues provides more accurate predictions of tumor biological behavior.[27] This approach offers clinicians a more reliable prognostic tool to optimize treatment strategies, improving patient survival rates and quality of life.[28] The peritumoral region plays a crucial role in tumor-host interactions, potentially influencing radiation-induced toxicity.[17] As post-radiotherapy tissue changes are a contributing factor to ETF formation, studying the peritumoral region can, to some extent, predict ETF occurrence.

Our choice of a 1 – 7 mm peritumoral expansion was based on anatomical and pathological considerations. In adults, the tracheal wall thickness ranges from 1 to 3 mm,[29] while the esophageal wall thickness is typically 2 – 5 mm, with an average of approximately 2.9 mm.[30,31] The maximal esophageal wall thickness during contraction is 4.70 mm (95% CI: 4.44 – 4.95 mm), while during expansion, it is 2.11 mm (95% CI: 2.00 – 2.23 mm). Therefore, the combined maximal thickness of the esophageal and tracheal walls is approximately 7 mm. As ETF arises from tumor invasion that breaches both walls, analyzing peritumoral zones within this range is biologically and clinically justified. Among the various peritumoral expansion intervals evaluated, the 2 mm expansion represents the critical zone where tumor infiltration may reach or breach the esophageal wall. This zone yielded the best predictive performance, suggesting that radiomic features in this region are most strongly associated with the development of ETF. Our peritumoral radiomics model, particularly features extracted from the 2 mm extension zone, showed incremental value when combined with intratumoral features. This aligns with the findings of Huang *et al.*,[25] where integrating peritumoral radiomics improved the

prediction of treatment response in colorectal cancer lung metastases. The peritumoral region may capture early tissue changes indicative of fistula formation, which might not be apparent within the tumor itself.

Our Combined model—integrating habitat radiomics, peritumoral radiomics, and clinical factors—achieved optimal predictive performance. This multifaceted approach provides a more comprehensive characterization of the tumor and its microenvironment. The Combined model potentially enables personalized radiotherapy planning and enhanced monitoring for high-risk patients. Our findings align with Wu *et al.*,[16] who developed a nomogram combining habitat radiomics and deep learning to predict epidermal growth factor receptor (EGFR) mutation in lung cancer, demonstrating the value of integrating multi-parametric radiomics in clinical decision-making.

Predicting ETF occurrence through our combined model not only stratifies high-risk groups but also allows for the optimization of radiation dose distribution through the analysis of imaging features. This approach can enhance treatment efficacy while reducing the incidence of severe adverse events like ETF.[32] Furthermore, our landmark analysis provided valuable insights into the temporal dynamics of risk stratification and survival among esophageal cancer patients following radiotherapy. By selecting a 5-month landmark—which corresponds to the average time for ETF onset—we minimized immortal time bias and temporally valid stratification. While the Combined model did not distinguish survival outcomes in the early phase posttreatment, it effectively stratified patients over the long term. This temporal pattern suggests that ETF may act as an intermediate event linking baseline risk to eventual survival outcomes. In summary, these findings highlight the value of our model for early identification of high-risk patients, enabling proactive intervention and potentially improving long-term survival. Furthermore, our study underscores the importance of accounting for temporal factors and potential mediators, such as ETF, in survival analyses.

This study has several limitations. Firstly, its retrospective nature and relatively small sample size may limit generalizability. Multi-center prospective validation is needed to further evaluate the robustness and applicability of our model across diverse populations and clinical settings. Secondly, we analyzed only pre-treatment CT images; incorporating longitudinal imaging during radiotherapy might provide additional predictive information. Thirdly, while we used habitat analysis to assess intratumoral heterogeneity, other advanced techniques like radiogenomics might offer further insights into the biological basis of ETF development. Additionally, we did not perform explicit batch-effect correction (e.g., ComBat harmonization) for radiomic features extracted from images acquired on two different CT scanners. Although standard preprocessing steps such as voxel resampling, gray-level normalization, and N4 bias field correction were performed—consistent with the majority of recent habitat radiomics studies[14-17]—subtle inter-scanner variability may exist. While our analyses did not detect significant scanner-related effects on radiomic features or model performance, we acknowledge that subtle inter-scanner variability may exist. Future studies, particularly multi-center efforts, may benefit from implementing more advanced harmonization techniques to enhance feature consistency. We also did not conduct additional uncertainty analyses, such as random contour erosion or dilation, to further assess the robustness of radiomic features to segmentation variability. This approach is consistent with the majority of recent habitat radiomics studies,[14-17] which typically focus on inter-observer ICC to assess reproducibility. Furthermore, the tumor ROIs in our study corresponded to GTVs defined for radiotherapy planning, which are routinely reviewed by senior clinicians to ensure treatment accuracy and safety. As such, the likelihood of significant inter-observer variability is extremely low within a single institution. Nevertheless, future studies could benefit from incorporating uncertainty analyses to further validate robustness, especially in multicenter or less standardized settings. Moreover, automated exclusion of adjacent organs, such as atlas-based or Boolean masks, was not performed in this study. Although the small expansion range (1 – 7 mm) and the manual trimming process minimized the risk of significant overlap with neighboring organs, automated methods may further reduce operator bias and improve reproducibility, especially for larger expansion margins or in multicenter studies. The lack of external validation from different institutions is another limitation of this study. Future multi-center collaborative efforts are needed to further validate our findings across diverse patient populations and treatment protocols.

## 5. Conclusion

In conclusion, this study demonstrates the potential of habitat-based and peritumoral radiomics in predicting post-radiotherapy ETF in esophageal cancer. The developed nomogram, integrating these advanced radiomics features with clinical factors, offers a promising tool for individualized risk stratification. Future work should focus on prospective validation, incorporation of multimodal and longitudinal imaging, and investigation of the biological mechanisms underlying the identified radiomics features.

## Acknowledgments

We thank all members of the guideline development group for their valuable contributions, especially the external reviewers for their insightful comments on the draft guidelines.

## Funding

This work was supported in part by the Chongqing Wanzhou Municipal Science and Health Joint Medical Research Project (Grant no.: wzstc-kw2023035).

## Conflict of interest

Mingzhu Yin is the Editor-in-Chief of this journal, but was not in any way involved in the editorial and peer-review process conducted for this paper, directly or indirectly. Separately, other authors declared that they have no known competing financial interests or personal relationships that could have influenced the work reported in this paper.

## Author contributions

*Conceptualization:* Zhuomiao Ye, Chao Deng, Mingzhu Yin
*Formal analysis:* Zhuomiao Ye
*Investigation:* Fei Xie, Longbin Zhang, YiQing Zhao
*Methodology:* Zhuomiao Ye
*Writing–original draft:* Zhuomiao Ye
*Writing–review & editing:* Zhuomiao Ye

## Ethics approval and consent to participate

This study was approved by the Ethics Committee of the Third Affiliated Hospital of Chongqing University (Chongqing Sanxia Hospital). The requirement for informed consent was waived because this study was a retrospective analysis utilizing medical records and/or biological specimens that were previously collected during routine clinical diagnosis and treatment, and posed minimal risk to the subjects.

## Consent for publication

Informed consent was waived by the Ethics Committee of the Third Affiliated Hospital of Chongqing University (Chongqing Sanxia Hospital) because this study was a retrospective analysis using data and/or images previously collected during routine clinical practice, and posed minimal risk to the participants.

## Availability of data

Data is available from the corresponding author upon reasonable request. Some data may not be made available because of privacy or ethical restrictions.

## References

1. Watanabe M, Toh Y, Ishihara R, *et al*. Comprehensive registry of esophageal cancer in Japan, 2015. *Esophagus*. 2023;20(1):1-28.
   doi: 10.1007/s10388-022-00950-5
2. Kumagai S, Koyama S, Shitara K. Precise patient stratification in esophageal cancer: Biomarkers for immunochemotherapy. *Cancer Cell*. 2023;41(7):1199-1201.
   doi: 10.1016/j.ccell.2023.06.004
3. Yoshinami Y, Nishimura E, Hosokai T, *et al*. Rare malignant neoplasm of the esophagus: Current status and future perspectives. *Jpn J Clin Oncol*. 2024;54(2):111-120.
   doi: 10.1093/jjco/hyad144
4. Xu YH, Lu P, Gao MC, Wang R, Li YY, Song JX. Progress of magnetic resonance imaging radiomics in preoperative lymph node diagnosis of esophageal cancer. *World J Radiol*. 2023;15(7):216-225.
   doi: 10.4329/wjr.v15.i7.216
5. Jha AK, Mithun S, Sherkhane UB, *et al*. Emerging role of quantitative imaging (radiomics) and artificial intelligence in precision oncology. *Explor Target Antitumor Ther*. 2023;4(4):569-582.
   doi: 10.37349/etat.2023.00153
6. Puttanawarut C, Sirirutbunkajorn N, Tawong N, *et al*. Radiomic and dosiomic features for the prediction of radiation pneumonitis across esophageal cancer and lung cancer. *Front Oncol*. 2022;12:768152.
   doi: 10.3389/fonc.2022.768152
7. Constanzo J, Wei L, Tseng HH, El Naga I. Radiomics in precision medicine for lung cancer. *Transl Lung Cancer Res*. 2017;6(6):635-647.
   doi: 10.21037/tlcr.2017.09.07
8. Zhu C, Liu J, Ke M, Yong Y, Luo B, Feng G. Hybrid stent in management of malignant airway obstruction with carina esophageal fistula: A case report. *Medicine (Baltimore)*. 2023;102(14):e33405.
   doi: 10.1097/MD.0000000000033405
9. Rieder F, Fiocchi C. Mechanisms of tissue remodeling in inflammatory bowel disease. *Dig Dis*. 2013;31(2):186-193.
   doi: 10.1159/000353364
10. Liu JZ, Zhong YS, Xu MD, Chen WF, Zhou PH, Yao LQ. [Membrane-covered self-expanding stents in the treatment of high-positioned esophageal stenosis or fistula]. *Zhonghua Wei Chang Wai Ke Za Zhi*. 2013;16(12):1146-1150.
11. Brunner S, Bruns CJ, Schroder W. [Esophagotracheal and esophagobronchial fistulas]. *Chirurg*. 2021;92(6):577-588.
   doi: 10.1007/s00104-021-01370-4

12. Nagore-Ancona JF, Acosta-Martinez A, Gonzalez-Luna JA, Martin-Perez JA, Sanchez-Baltazar AL, Perna-Lozada L. Surgical approach for iatrogenic tracheoesophageal fistula. Case report and literature review. *Cir Cir*. 2021;89(6): 811-817.

doi: 10.24875/ciru.20000730

13. Amin MB, Greene FL, Edge SB, *et al*. *AJCC Cancer Staging Manual*. 8th ed. Berlin: Springer; 2017.

14. Yuan J, Wu M, Qiu L, *et al*. Tumor habitat-based MRI features assessing early response in locally advanced nasopharyngeal carcinoma. *Oral Oncol*. 2024;158:106980.

doi: 10.1016/j.oraloncology.2024.106980

15. Bi Q, Miao K, Xu N, *et al*. Habitat radiomics based on MRI for predicting platinum resistance in patients with high-grade serous ovarian carcinoma: A multicenter study. *Acad Radiol*. 2024;31(6):2367-2380.

doi: 10.1016/j.acra.2023.11.038

16. Wu J, Meng H, Zhou L, *et al*. Habitat radiomics and deep learning fusion nomogram to predict EGFR mutation status in stage I non-small cell lung cancer: A multicenter study. *Sci Rep*. 2024;14(1):15877.

doi: 10.1038/s41598-024-66751-1

17. Huang H, Chen H, Zheng D, *et al*. Habitat-based radiomics analysis for evaluating immediate response in colorectal cancer lung metastases treated by radiofrequency ablation. *Cancer Imaging*. 2024;24(1):44.

doi: 10.1186/s40644-024-00692-w

18. Liu Y, Li Z, Xiong H, Gao X, Wu J, Wu S. Understanding and enhancement of internal clustering validation measures. *IEEE Trans Cybern*. 2013;43(3):982-994.

doi: 10.1109/tsmcb.2012.2220543

19. Hurtgen M, Herber SC. Treatment of malignant tracheoesophageal fistula. *Thorac Surg Clin*. 2014;24(1):117-127.

doi: 10.1016/j.thorsurg.2013.09.006

20. Choi MK, Park YH, Im YH, *et al*. Clinical implications of esophagorespiratory fistulae in patients with esophageal squamous cell carcinoma. *Med Oncol*. 2010; 27: 1234-1238.

doi: 10.1007/s12032-009-9364-z

21. Balazs A, Kupcsulik PK, Galambos Z. Esophagorespiratory fistulas of tumorous origin. Non-operative management of 264 cases in a 20-year period. *Eur J Cardiothorac Surg*. 2008;34(5):1103-1107.

doi: 10.1016/j.ejcts.2008.06.025

22. Noronha V, Joshi A, Patil VM, *et al*. Efficacy and safety of induction chemotherapy in esophageal cancer with airway involvement. *J Gastrointest Cancer*. 2016;47(3):294-304.

doi: 10.1007/s12029-016-9830-8

23. Wang H, Zhang L, Liu W. Tracheoesophageal fistula caused by successful response to pembrolizumab in a patient with squamous cell lung cancer. *J Thorac Oncol*. 2019;14(7):e141-e143.

doi: 10.1016/j.jtho.2019.02.013

24. Jeong SY, Park JE, Kim N, Kim HS. Hypovascular cellular tumor in primary central nervous system lymphoma is associated with treatment resistance: Tumor habitat analysis using physiologic MRI. *AJNR Am J Neuroradiol*. 2022;43(1):40-47.

doi: 10.3174/ajnr.A7351

25. Napel S, Mu W, Jardim-Perassi BV, Aerts HJ, Gillies RJ. Quantitative imaging of cancer in the postgenomic era: Radio(geno)mics, deep learning, and habitats. *Cancer*. 2018;124(24):4633-4649.

doi: 10.1002/cncr.31630

26. Caii W, Wu X, Guo K, Chen Y, Shi Y, Chen J. Integration of deep learning and habitat radiomics for predicting the response to immunotherapy in NSCLC patients. *Cancer Immunol Immunother*. 2024;73(8):153.

doi: 10.1007/s00262-024-03724-3

27. Yuda Handaya A, Anwar SL, Fauzi AR, Werdana VA. Sweat gland tumor microenvironment. *Adv Exp Med Biol*. 2020;1296:259-274.

doi: 10.1007/978-3-030-59038-3_16

28. Huang YC, Huang SM, Yeh JH, *et al*. Utility of CT radiomics and delta radiomics for survival evaluation in locally advanced nasopharyngeal carcinoma with concurrent chemoradiotherapy. *Diagnostics (Basel)*. 2024;14(9):941.

doi: 10.3390/diagnostics14090941

29. Webb EM, Elicker BM, Webb WR. Using CT to diagnose nonneoplastic tracheal abnormalities: Appearance of the tracheal wall. *AJR Am J Roentgenol*. 2000;174(5):1315-1321.

doi: 10.2214/ajr.174.5.1741315

30. Berkovich GY, Levine MS, Miller WT Jr. CT findings in patients with esophagitis. *AJR Am J Roentgenol*. 2000;175(5):1431-1434.

doi: 10.2214/ajr.175.5.1751431

31. Xia F, Mao J, Ding J, Yang H. Observation of normal appearance and wall thickness of esophagus on CT images. *Eur J Radiol*. 2009;72(3):406-411.

doi: 10.1016/j.ejrad.2008.09.002

32. Ger RB, Wei L, Naqa IE, Wang J. The promise and future of radiomics for personalized radiotherapy dosing and adaptation. *Semin Radiat Oncol*. 2023;33(3):252-261.

doi: 10.1016/j.semradonc.2023.03.003